



**HAL**  
open science

## Very Long-Lived Photogenerated High-Spin Phase of a Multistable Spin-Crossover Molecular Material

Teresa Delgado, Antoine Tissot, Laure Guénée, Andreas Hauser, Francisco Javier Valverde-Muñoz, Maksym Seredyuk, José Antonio Real, Sébastien Pillet, El-Eulmi Bendeif, Céline Besnard

### ► To cite this version:

Teresa Delgado, Antoine Tissot, Laure Guénée, Andreas Hauser, Francisco Javier Valverde-Muñoz, et al.. Very Long-Lived Photogenerated High-Spin Phase of a Multistable Spin-Crossover Molecular Material. *Journal of the American Chemical Society*, 2018, 140 (40), pp.12870-12876. <10.1021/jacs.8b06042>. <hal-02314062>

**HAL Id: hal-02314062**

**<https://hal.science/hal-02314062v1>**

Submitted on 7 Dec 2023

HAL is a multi-disciplinary open access archive for the deposit and dissemination of scientific research documents, whether they are published or not. The documents may come from teaching and research institutions in France or abroad, or from public or private research centers.

L'archive ouverte pluridisciplinaire HAL, est destinée au dépôt et à la diffusion de documents scientifiques de niveau recherche, publiés ou non, émanant des établissements d'enseignement et de recherche français ou étrangers, des laboratoires publics ou privés.



HAL Authorization

# Very long-lived photogenerated high-spin phase of a multistable spin-crossover molecular material

Teresa Delgado,<sup>[a]</sup> Antoine Tissot,<sup>[b]</sup> Laure Guénée,<sup>[c]</sup> Andreas Hauser,<sup>[a]</sup> Francisco Javier Valverde-Muñoz,<sup>[d]</sup> Maksym Seredyuk,<sup>[d]</sup> José Antonio Real\*,<sup>[d]</sup> Sébastien Pillet,<sup>[e]</sup> El-Eulmi Bendeif<sup>[e]</sup> and Céline Besnard\*<sup>[c]</sup>

a. Département de Chimie Physique, Université de Genève, 1211 Genève, Switzerland.

b. Institut des Matériaux Poreux de Paris, FRE 2000 CNRS, Ecole Normale Supérieure, Ecole Supérieure de Physique et de Chimie Industrielle de Paris, PSL Research University, 75005 Paris, France.

c. Laboratoire de Cristallographie, Université de Genève, 1211 Genève, Switzerland.

d. Departament de Química Inorgànica, Institut de Ciència Molecular (ICMol), Universitat de València, Valencia, Spain

e. Université de Lorraine, CNRS, CRM2, Nancy, France

*spin crossover • LIESST • relaxation dynamics • nucleation and growth phenomena • cooperative effect*

---

**ABSTRACT:** The spin-crossover compound  $[\text{Fe}(\text{n-Bu-im})_3(\text{tren})](\text{PF}_6)_2$  shows an unusual long relaxation time of 20 h after light-induced excited spin state trapping (LIESST) when irradiating at 80 K. This is more than 40 times longer than when irradiating at 10 K. Optical absorption spectroscopy and X-ray diffraction using synchrotron radiation were used to characterize and compare the LIESST behavior of this compound after irradiation at around 10 K and 80 K. Rearrangement of the butyl chains of the ligands occurring during the relaxation after irradiation at 80 K are thought to be responsible for the unusually long relaxation time at this temperature.

---

## INTRODUCTION

Responsive switchable materials have always attracted widespread attention because they afford excellent study examples for the understanding of mechanisms involved in phase transitions and provide opportunities for future and emerging technologies.<sup>1-3</sup>

Some of the most investigated switchable molecular materials are pseudo-octahedral iron(II) spin-crossover (SCO) complexes. They reversibly switch between the high-spin (HS,  $t_{2g}^4 e_g^2$ ) and low-spin (LS,  $t_{2g}^6 e_g^0$ ) electronic states by the action of external stimuli (temperature, pressure, light and analytes). Given the antibonding nature of the  $e_g$  orbitals, the HS $\leftrightarrow$ LS conversion is accompanied by changes in Fe-ligand bond lengths and angles, which confer bistability (memory) to the magnetic, optical, dielectric, structural and mechanical properties, when elastic interactions between the SCO centers favor strong cooperativity in the crystal.<sup>4-6</sup> This appealing feature can be combined with other relevant properties such as luminescence, electronic transport, chirality or host-guest chemistry in a synergetic fashion, thereby transferring their intrinsic bistable nature to the second property, thus resulting in multifunctional materials that can be processed at different levels, from bulk to single molecules.<sup>7-8</sup>

These important attributes have created solid expectancies for the generation of sensors, actuators and spintronic devices

based on the on-off switching properties of the SCO materials.<sup>9-14</sup> In this context, light is a desirable channel for triggering the HS $\leftrightarrow$ LS switch since it may improve flexibility and storage density in such devices.<sup>1-3</sup> In fact, it is possible to achieve a quantitative LS $\rightarrow$ HS conversion in Fe<sup>II</sup> SCO complexes by irradiating the sample in the UV-Vis or near-IR regions at low temperature, typically at 10 K. This phenomenon is known as "light-induced excited spin state trapping" (LIESST).<sup>15</sup> The lifetime of the photogenerated metastable HS state is inversely proportional to the thermal SCO temperature,  $T_{1/2}$ , at which the molar HS and LS fractions are equal to 0.5 and the Gibbs free energy difference  $\Delta G_{HL}$  is equal to 0.<sup>16-17</sup> The kinetic stability of the photogenerated HS state can be roughly estimated following a precise protocol which determines the characteristic temperature  $T_{LIESST}$  at which the photogenerated HS state relaxes to the LS state within a few minutes.<sup>18</sup> The goal is to correlate  $T_{LIESST} - T_{1/2}$  data with relevant structural parameters that may help chemical design aiming at increasing  $T_{LIESST}$  towards room temperature. The  $\text{FeN}_6$  core, determined by the nature of the ligands, plays a crucial role in the magnitude of  $T_{LIESST}$ .<sup>18</sup> In pure SCO compounds  $T_{LIESST}$  values are usually in the interval 20 - 100 K.

On the other hand crystallographic studies are crucial to provide the knowledge of the structural rearrangements occurring during the spin transition.<sup>19</sup> Different kinds of phase transitions

can accompany the spin crossover. For example, order-disorder transitions originating from the counter anions,<sup>20-23</sup> the solvent<sup>24-27</sup> or some part of the ligand.<sup>22, 28-30</sup>

[Fe(n-Bu-im)<sub>3</sub>tren](PF<sub>6</sub>)<sub>2</sub>, (n-Bu-im)<sub>3</sub>(tren) = n-butyl imidazoltris(2-ethylamino)amine has a complex SCO behavior previously studied by magnetic measurements. Two different SCO behaviors have been observed depending on the sweeping rate of the temperature.<sup>31</sup> For a scan rate of 4 K/min, the SCO between the HS and the LS phase (called LS<sub>1</sub>) is characterized by an average critical temperature of 122 K with a hysteresis loop of 14 K, while for a slower scan rate of 0.1 K/min the SCO between the HS phase and a different LS phase (called LS<sub>2</sub>) is characterized by an average critical temperature of 156 K and a hysteresis loop of 41 K. For intermediate scan rates, coalescence of the two hysteric behaviors is observed. The phase transition occurring between the HS and LS states involves several conformational changes of the butyl chains of the substituent of the ligand. Besides the usual HS to LS FeN<sub>6</sub> coordination sphere rearrangements, the HS and LS<sub>1</sub> structures only differ by moderate structural modifications. The HS and LS<sub>2</sub> structures, on the other hand, strongly differ from each other in the orientation of several butyl groups and of the counter anions. In other words, the two different LS phases, LS<sub>1</sub> and LS<sub>2</sub>, present remarkable structural differences. Consequently, the crystal packing is different due to different C...F contacts between the complex and the PF<sub>6</sub><sup>-</sup> groups. In the HS phase, only one discreet C...F interaction is produced, whereas in the case of the LS<sub>1</sub> and LS<sub>2</sub> phases, many interactions are present.

Herein, the scan rate dependence of the thermal spin transition of [Fe(n-Bu-im)<sub>3</sub>tren](PF<sub>6</sub>)<sub>2</sub> is confirmed and the LIESST behavior of the LS<sub>1</sub> and LS<sub>2</sub> phases investigated by single crystal optical absorption spectroscopy measurements and X-ray diffraction. Irradiating LS<sub>1</sub> below 70 K quantitatively photogenerates a HS state which relaxes within half an hour at 80 K. Unexpectedly, irradiating LS<sub>1</sub> at the relatively high temperature of 80 K quantitatively photogenerates another HS state which relaxes unusually slowly, in around 20 h. The structures of both HS states were characterized by single-crystal diffraction and the structural rearrangements explaining the long relaxation after irradiation above 70 K were monitored by synchrotron single-crystal X-ray diffraction.

## EXPERIMENTAL METHODS

### Single crystal optical absorption spectroscopy.

Single crystals of [Fe(n-Bu-im)<sub>3</sub>tren](PF<sub>6</sub>)<sub>2</sub> were mounted on a copper plate with a previously drilled hole of approximately 15 μm in diameter. One crystal was deposited in the middle of the hole and fixed with silver paste to ensure a good thermal conductivity. The sample was then introduced into a closed cycle cryostat (Janis-Sumimoto SHI-4.5), which operates between 4 and 300 K and is equipped with a programmable temperature controller (Lakeshore Model 331). The cryostat was introduced into a double beam spectrometer (Varian Cary 5000).

In all experiments, a LS reference spectrum was first collected at 10 K. Then the sample was irradiated with a 690 nm laser, which corresponds to the tail of the LS band centered at 669

nm, during 10 min at 10 mW/mm<sup>2</sup>, and a reference HS spectrum was recorded likewise at 10 K. The HS fraction ( $\gamma_{HS}$ ) was obtained using equation 1.

$$\gamma_{HS} = (OD_{LS} - OD_T) / (OD_{LS} - OD_{HS}), \quad (1)$$

where OD<sub>LS</sub> is the optical density of the LS state, OD<sub>HS</sub> is the optical density of the HS state at 10 K and OD<sub>T</sub> is the optical density at a given temperature. The optical density (OD) is corrected from an eventual baseline jump or shift by taking the difference between the OD at 600 nm and the OD at 750 nm, where there is no noticeable absorption in the two states.

In the case of the LIESST experiment, after irradiation at 10 K, the temperature was quickly raised to the desired temperature for the relaxation measurement (at about 20 K/min) and spectra were then recorded in appropriate time intervals during the relaxation. In the case of the LIESST experiment at 80 – 100 K, the irradiation and the relaxation was performed at the same temperature. In these cases  $\gamma_{HS}$  is calculated using equation 1 but replacing OD<sub>T</sub> by OD<sub>t</sub>, that is, the optical density at a given time during the relaxation.

### Synchrotron-based X-ray diffraction.

The thermal and photo-induced spin transitions were studied using X-ray diffraction at the Swiss Norwegian Beamline at the European Synchrotron Radiation Facility in Grenoble (France). The same diffractometer equipped with a 2D PILATUS2M detector, was used for single crystal and powder diffraction experiments. The temperature was controlled using an Oxford Cryostream 700. All the samples (single crystals and powders) were placed in Mitegen Kapton loops.

For single crystals: 360° phi-rotations of 6 min each were collected. Data were integrated with CryAlis Pro.<sup>32</sup> Further X-ray data analyses were carried out using the Olex<sup>2</sup> Crystallography Software<sup>33</sup> and Shelxl.<sup>34</sup> For the relaxation experiment, the samples were irradiated at 90 K with a DPSS 690 nm laser during around 10 minutes at 10 mW/mm<sup>2</sup>.

For powders: the powder was obtained by carefully crushing a few single crystals of [Fe(n-Bu-im)<sub>3</sub>tren](PF<sub>6</sub>)<sub>2</sub>. For the thermal transition, the scan rate was 4 K/min. The relaxation was followed by recording diffraction patterns every 22 s. The 2D data were integrated using the SNBL-home-made software BUBBLE.<sup>35</sup> Further X-ray data analyses were carried out using the Topas academic software.<sup>36</sup>

### Home-lab X-ray diffraction.

The single crystal diffraction data for the 10 K thermally quenched and 125 K thermally quenched states were collected with an Oxford Diffraction SuperNova diffractometer equipped with an Atlas CCD detector, an helium open flow cryosystem (Oxford Diffraction Helijet) or a nitrogen cryostream cooling device. The unit-cell determination and data reduction were performed using the CryAlis Pro<sup>32</sup> program suite on the full data set. An analytical absorption correction was carried out. The crystal structures were refined on  $F^2$  by weighted full-matrix least-squares methods using the SHELXL97 program.<sup>34</sup>

The 25 K diffraction data was collected using a Nonius Kappa CCD diffractometer equipped with a Helix He cryosystem. In a first step, the small size (100  $\mu\text{m}$ ) single crystal sample was quickly cooled to 120 K, then slowly down to 25 K in the  $\text{LS}_1$  state. A complete data set on the  $\text{LS}_1$  state was recorded at 25K. The sample was then irradiated with a laser at 532 nm (laser power of 10 mW, enlarging the beam to ensure a homogeneous irradiation) for 1 hour while continuously rotating the crystal, and a complete data set on the HS state was then recorded. The diffraction data were integrated and reduced using the HKL package.<sup>37</sup> An empirical absorption correction was applied. The crystal structures were refined on  $F^2$  by weighted full-matrix least-squares methods using the *SHELXL97* program.<sup>34</sup>

## RESULTS AND DISCUSSION

### Thermal spin transition.

Crystals of around  $20 \pm 1 \mu\text{m}$  thickness were used for all the measurements. The dependence of the thermal spin transition behavior with the scan rate of the temperature observed by Real *et al.*<sup>31</sup> was confirmed by absorption spectroscopy measurements (see Figure S1 in Supporting Information for more details) and powder diffraction measurements (Figure S2). By looking more carefully at the 3D plots of the powder diffraction measurements, it is possible to observe that the transition is mainly associated with an intensity change of the HS and LS peaks without large shifts of the peaks in both heating and cooling. This can be associated with a nucleation and growth phenomenon.<sup>38</sup> Furthermore, the  $\text{HS} \rightarrow \text{LS}_2$  thermal relaxation was followed by optical spectroscopy at different temperatures around the  $\text{HS-LS}_2$  thermal transition. This confirmed that the relaxation rate decreases with the temperature, which is in line with a first order phase transition.<sup>39</sup> The relaxation is strongly sigmoidal due to the kinetics of the crystallographic phase transition reflecting the nucleation and growth mechanism (Figure S3).

### Kinetics of the photo-induced $\text{HS} \rightarrow \text{LS}_1$ relaxation

*Kinetics of the  $\text{HS} \rightarrow \text{LS}_1$  relaxation after irradiation of the  $\text{LS}_1$  phase at 10 K followed by absorption spectroscopy.*

The  $\text{LS}_1$  phase was obtained using a cooling rate of 4 K/min. The absorption spectrum collected after irradiation at 10 K corresponds to a pure HS state (Figure S4a). Considering the  $T_{\text{LIESST}}(\text{HS})$  value of 79.8 K (Figure S14a), we selected 6 temperatures for the relaxation: 80, 77.5, 75, 72.5, 70, 65 and 60 K. For all the temperatures, a plateau is present in the relaxation curves when the HS fraction is around 0.5 (Figure 1 and Figure S7). This can be due to a specific structural reorganization, which could be, for example, an ordering of the HS and LS state.<sup>24, 40</sup> Evidently, the mean-field approach is not appropriate in this case. Instead, average relaxation rate constants were taken from the time necessary to relax to  $\gamma_{\text{HS}} = 0.5$ . The linear evolution of  $\ln k_{\text{HL}}$  vs  $1/T$  indicates that the relaxation from the photo-induced HS state to the ground state  $\text{LS}_1$  is quasi thermally activated (Figure S5a). An activation energy of 10.2 kJ/mol ( $850 \text{ cm}^{-1}$ ) was extracted from the slope of the Arrhenius plot. This indicates that we are in a transition regime between low-temperature tunneling and classical behaviour.<sup>41</sup>

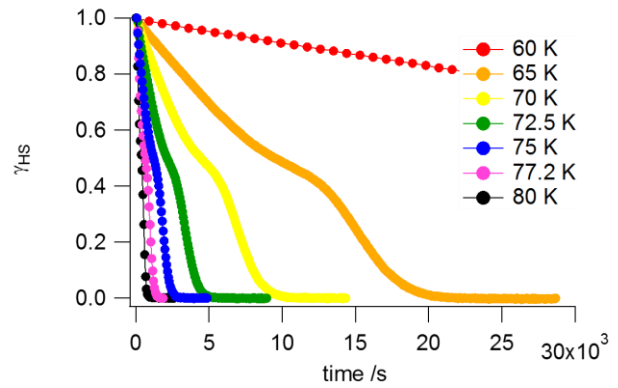


**Figure 1.** Evolution of the normalized photo-induced HS fraction as a function of time at various temperatures for the  $\text{HS} \rightarrow \text{LS}_1$  relaxation after irradiation of the  $\text{LS}_1$  phase. All the experiments start from a quantitative population of the HS state at 10 K followed by a relaxation at the indicated temperature.

*Kinetics of the photo-induced  $\text{HS} \rightarrow \text{LS}_1$  relaxation after irradiation of the  $\text{LS}_1$  phase around  $T_{\text{LIESST}}$  followed by magnetometry and absorption spectroscopy.*

The relaxation was studied at 80K after irradiations at 45 K, 65 K, 70 K and 75 K (magnetometry) and 80 K (absorption spectroscopy). Figure 2 shows the obtained relaxation curves. Surprisingly, for irradiation temperatures above 65 K the relaxations at 80 K get slower. Irradiating at 80 K leads to a relaxation time close to 20 h - more than 40 times the relaxation time observed when irradiating at 10 K (Figure S8b) - with a very long nucleation process of around 14 h. The relaxation curve is very sigmoidal, with a kink observed at a HS fraction of around 0.4. Experiments were also performed by absorption spectroscopy with irradiation and relaxation at 80 K, 87 K, 90 K and 100 K (Figure S8c). At 87 K, the process is considerably faster (total relaxation time 11 h, nucleation time 4 h) and a second step is observed after approximately 5 h when the HS fraction is around 0.6. At 90 K, and 100 K the plateau can be still observed, and the relaxation becomes faster when the temperature increases.

In summary, irradiation at temperatures above 65K of the  $\text{LS}_1$  phase leads to unexpected long  $\text{HS} \rightarrow \text{LS}_1$  relaxation times. The relaxation curves show a plateau for HS fraction of around 0.4 and a small change in the irradiation and relaxation temperature can drastically change the relaxation time.

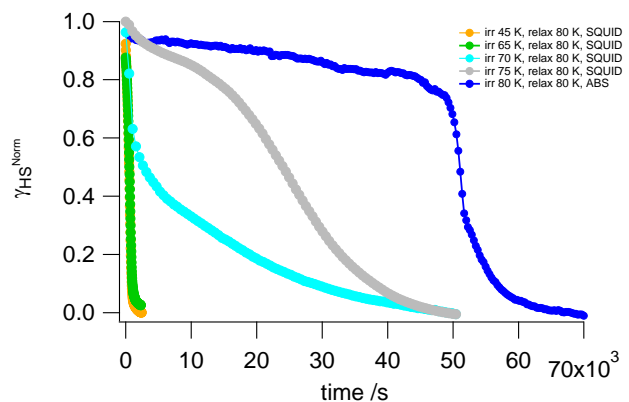


**Figure 2.** Evolution of the normalized photo-induced HS fraction as a function of time at 80K for the HS  $\rightarrow$ LS<sub>1</sub> relaxation after irradiation of the LS<sub>1</sub> phase at temperatures from 45 to 80 K at 690 nm at 10 mW/mm<sup>2</sup> during 10 min. All the experiments start from a quantitative population of the HS state by irradiation at the indicated temperature followed by a relaxation at 80 K

### Structural studies

In order to understand the different relaxation behaviors for the LIESST HS state generated below and above 70 K from the LS<sub>1</sub> phase, structural investigations were carried out using single crystal X-ray diffraction. In particular the butyl chains of the ligands, which adopt different conformations in the already characterized LS<sub>1</sub>, LS<sub>2</sub> and HS states, were closely examined.

A LS<sub>1</sub> structure was obtained at 25 K.<sup>42</sup> identical to the one reported at 110K.<sup>31</sup> The sample was then irradiated with a 532 nm laser for 1 hour while continuously rotating the crystal and an HS structure was obtained (Table S1). The HS state structure of the irradiated sample at 25 K, which we will call HS<sub>1</sub><sup>1irr</sup>, presents a complete ordering of all the alkyl substituents, in the same conformation as in the LS<sub>1</sub> state. There is no noticeable change in the geometry of the ligands between the LS<sub>1</sub> and HS<sub>1</sub><sup>1irr</sup> structures, except some structural rearrangements induced by the different Fe-N bond lengths between the two spin states (Figure S9, superposition).

Using a liquid-nitrogen cooler, a LS<sub>1</sub> structure was recorded around 90 K, it is very similar to the LS<sub>1</sub> structure determined at 25K (Figure S10, superposition).<sup>43</sup> The sample was then irradiated at 690 nm with 10 mW/mm<sup>2</sup> during 10 min and the structure of the metastable HS excited state that we will call HS<sub>1</sub><sup>2irr</sup> was subsequently determined. The structures of HS<sub>1</sub><sup>1irr</sup> and HS<sub>1</sub><sup>2irr</sup> differ: in HS<sub>1</sub><sup>2irr</sup>, one of the butyl chains is disordered and another butyl chain is in a different conformation compared to the structure of LS<sub>1</sub> or HS<sub>1</sub><sup>1irr</sup>. (Figure S11, superposition).

The HS<sub>1</sub><sup>2irr</sup>  $\rightarrow$ LS<sub>1</sub> relaxation was also monitored by single-crystal X-ray diffraction at 90 K after photo-excitation. The time evolution of the HS fraction was calculated through Vegard's law on the Fe-N bond length (Equation 2).

$$V_{\text{HS}}(t) = \frac{r_{(\text{Fe-N})}(t) - r_{(\text{Fe-N})_{\text{LS}}}}{r_{(\text{Fe-N})_{\text{HS}}} - r_{(\text{Fe-N})_{\text{LS}}}}, \quad (2)$$

where  $r_{(\text{Fe-N})}(t)$  is the average Fe-N distance at the time  $t$ ,  $r_{(\text{Fe-N})_{\text{HS}}}$  is the average Fe-N distance of the HS state at 90 K (obtained under continuous irradiation) and  $r_{(\text{Fe-N})_{\text{LS}}}$  is the average Fe-N distance of the LS<sub>1</sub> state at 90 K. The corresponding used Fe-N bond length and unit-cell parameters obtained for all the structures taken during the relaxation are summarized in Table S3. The relaxation curve obtained by single crystal diffraction is compared to the relaxation curves obtained by absorption spectroscopy in Figure S8d. The relaxation time indicates a temperature of around 90 K.

The structures during the relaxation are shown in Figure 3 alongside with the obtained relaxation curve. In the photoinduced HS<sub>1</sub><sup>2irr</sup> state, the butyl chain of one ligand is disordered (chain A) with two randomly distributed orientations (red and violet chains). The other butyl chains (B and C) are ordered. After cutting off the laser irradiation, the relaxation proceeds very slowly for approximately 1 h. During this nucleation time, disorder grows on chain B (green and orange chains). As the relaxation becomes faster, chain A orders in one of its initial orientations (red). Chain B also starts to order, flipping its initial orientation (from the initial orange chain to the final green one). Clearly, this order/disorder phase transition that takes place in two different butyl groups of the ligands is directly related with the kink observed in the middle of the relaxation and with the long relaxation time. The rearrangements of the structure create different interactions patterns between the butyl groups and the counter anions, especially through the H (butyl) – F(PF<sub>6</sub><sup>-</sup>) bonds (Tables S4-S5).

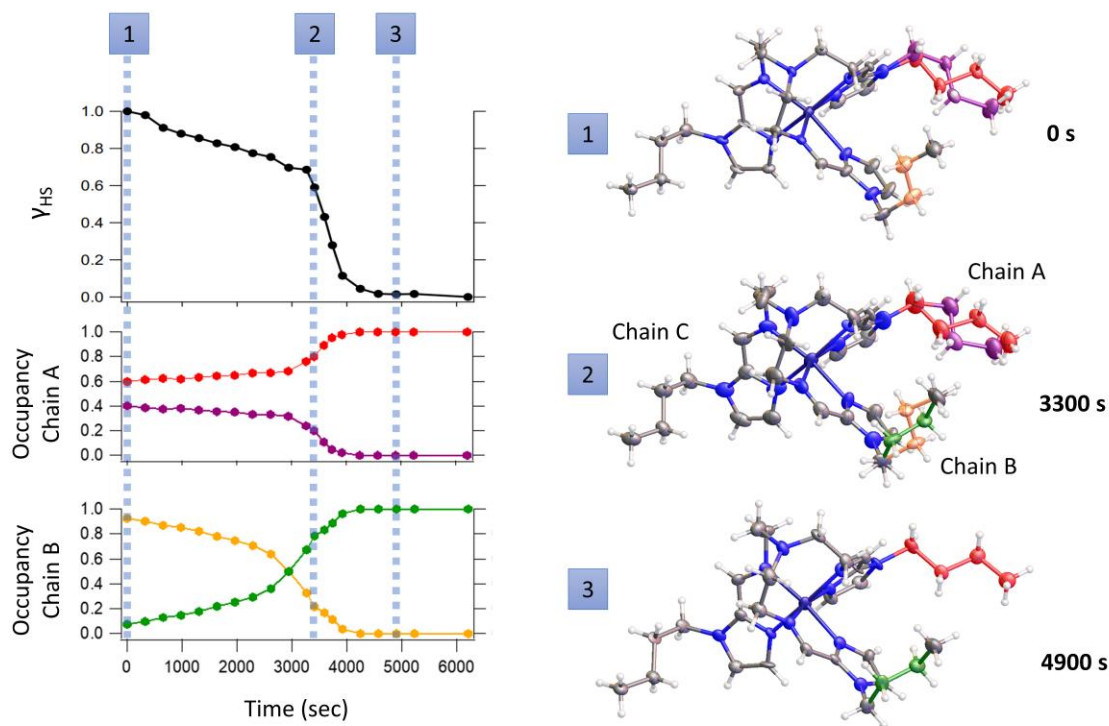


**Figure 3.** Relaxation curve obtained by single crystal X-ray diffraction using synchrotron radiation at 90 K after irradiation at the same temperature of the  $LS_1$  phase. The HS fraction curve (black) is derived from the crystallographic Fe-N distances. The structure of the complex is shown at three different relaxation times on this curve, with displacement ellipsoids depicted at 40 percent probability level. An order/disorder phase transition takes place in two different butyl groups of the ligand, chain A and B during the relaxation from  $HS_1^{2irr}$  to  $LS_1$ . For each chain two different positions of the butyl group are observed, represented with different colors. The occupancy factor defines the proportion of the chain being in the given position. The evolutions with time of the occupancy factors for chain A and chain B are shown below the relaxation curve.

Alternatively, the unexpected long-time scale of the  $HS_1^{2irr} \rightarrow LS_1$  relaxation was also monitored by magnetic measurements (Figure S15) and synchrotron-based X-ray powder diffraction (Figure S16). The timescale of the relaxation obtained by both techniques are similar to the one observed on single crystals. However, the nucleation time is decreased and the relaxation speeds up compared to single crystal XRD (Table S6 summarizes the different relaxation time obtained by the different measurements).

The differences observed between the different measurement techniques can be attributed to the sample preparation. Indeed, the crushing of the crystals to produce powdered samples affects the crystal quality. We have also observed that the exact shape of the relaxation curve differs slightly from crystal to crystal. Two relaxation cycles on the same crystal gave reproducible results (Figure S17 and Figure S8e). However, as shown in Figure S8e, we observed different relaxation curves on the same crystal after irradiation at 90 K when going back to room temperature and cooling again to 90 K in between the irradiations. Cycling to room temperature induces cracks and

defects in the crystals, reducing the size of the domains, which cancels the long nucleation time during which chain B is slowly disordering. As a consequence, the relaxation time is shortened.

Finally, quenching of the HS phase by quickly lowering the temperature gave a  $HS^{quench}$  phase whose structure is similar to  $HS_1^{2irr}$ . The relaxation of this quenched phase was studied by magnetic measurements and the relaxation time is of the same order of magnitude than the photo-excited  $HS_1^{2irr}$  phase (Figure S18). This is expected as the same rearrangement of the butyl chains has to occur during the relaxation.

In Figure 4, the structural diagram of the different HS and LS states, whose structures are elucidated, is presented. This system is a very nice example of how multistability can influence the spin crossover properties. Two low spin states are observed for different cooling rates. Two HS states are also observed at low temperature, one that can be reached by irradiation below 70 K and one that can be reached either by irradiation above 70 K or quenching of the room temperature HS state. The reorganization of the butyl side chains between these states governs the LIESST relaxation.

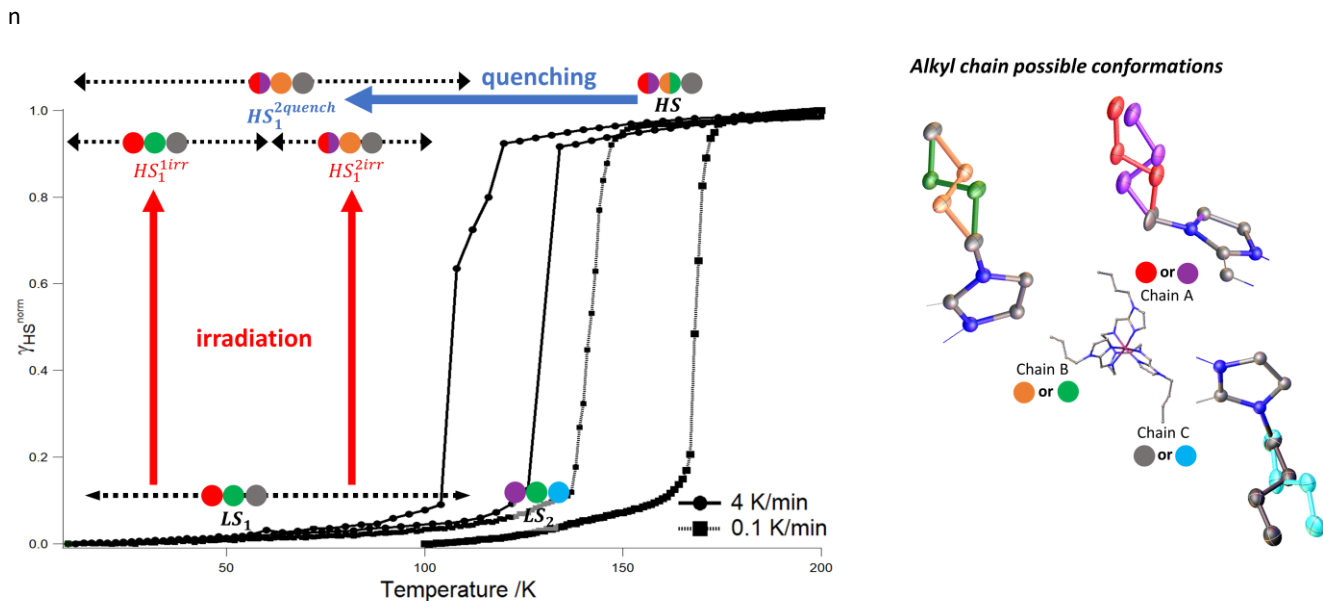


**Figure 4** Simplified structural diagram of  $[\text{Fe}(\text{n-Bu-im})_3\text{tren}](\text{PF}_6)_2$ ;  $(\text{n-Bu-im})_3(\text{tren}) = \text{n-butyl imidazoltris}(2\text{-ethylamino})\text{amine}$ . The different conformations that the alkyl chains can adopt are shown on the right. For each phase of the phase diagram, three colored disks indicate the positions adopted by chain A, B and C. Two-colored disks indicate that the chain is disordered over both positions. For the quenched phases, a small disorder on chain B is sometimes observed, depending on the temperature, but only the main conformation of the chain has been indicated (see table S7a).

### Kinetics of the photo-induced $\text{HS} \rightarrow \text{LS}_2$ relaxation

*Kinetics of the  $\text{HS} \rightarrow \text{LS}_2$  relaxation after irradiation of the  $\text{LS}_2$  phase at 10 K followed by absorption spectroscopy.* The  $\text{LS}_2$  phase was obtained using a cooling rate 0.1 K/min. The spectrum collected after irradiation at 10 K corresponds to a pure HS state (Figure S4b). Considering the  $T_{\text{LIESST}}(\text{HS}_2)$  value of 50 K (Figure S14b), six temperatures for the relaxation were selected: 55, 50, 45, 40, 35 and 30 K. The relaxation curves show a slightly sigmoidal behavior (Figure 5). Therefore, they were fitted within the framework of the mean-field model,<sup>44</sup> with the relaxation rate constant  $k_{\text{HL}}$  depending not only on the temperature but also on the LS fraction (Equation 3) in such a way that in the differential equation of  $d\gamma_{\text{HS}}/dt$ , a new term that accounts for the cooperative effects is introduced (Equation 4).

$$k_{\text{HL}}(T, \gamma_{\text{HS}}) = k_{\text{HL}}(T, \gamma_{\text{HS}} = 0) e^{\alpha \gamma_{\text{LS}}} , \quad (3)$$

$$\frac{d\gamma_{\text{HS}}}{dt} = -k_{\text{HL}}^0 \cdot e^{-\frac{E_a}{k_B T}} \cdot e^{\alpha (1-\gamma_{\text{HS}})} \cdot \gamma_{\text{HS}} , \quad (4)$$

In equation (3)  $k_{\text{HL}}^0$  is the relaxation rate constant and  $E_a$  the activation energy at the beginning of the relaxation, and  $\alpha$  is the acceleration factor.  $k_{\text{HL}}^0$  was obtained from the slope of the relaxation curve considering only the first relaxation points, that is, between  $t = 0$  and  $t \approx 1000$  s. The apparent  $E_a$  value was then calculated from the slope of an Arrhenius plot (Figure S5b). The resulting value for  $E_a$  of 3.3 kJ/mol ( $276 \text{ cm}^{-1}$ ) is rather small and indicates that in the temperature interval from 30 to 55 K we are only just above the low-temperature tunneling regime. This is also borne out by the slight curvature of the Arrhenius plot. The above value of  $E_a$  has subsequently been

introduced into equation 3 in order to obtain the value of  $\alpha$  via least squares numerical fitting. The calculated value of  $\alpha$  is 1.5 at 35 K (Figure S6) and corresponds to a moderately cooperative relaxation curve. It should be noted that towards the end of the relaxation curve, the experimental data deviate quite strongly from the calculated mean-field curve. Such a behavior, with a long tail, is indicative of a comparatively large inhomogeneous distribution of activation energies.<sup>44</sup> Overall, the  $\text{HS} \rightarrow \text{LS}$  relaxation after irradiation of the  $\text{LS}_2$  phase (irradiation at 10 K) is faster than the  $\text{HS} \rightarrow \text{LS}$  relaxation after irradiation of the  $\text{LS}_1$  phase (irradiation at 10 K). This can be directly correlated with the thermal transition temperature, which is higher for  $\text{LS}_2$  (see Figure S1).

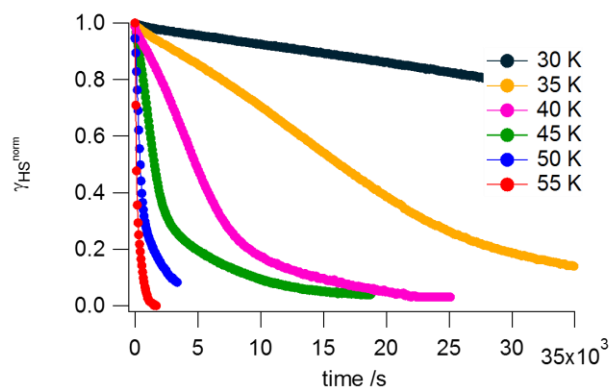


**Figure 5.** Evolution of the normalized photo-induced HS fraction as a function of time at various temperatures for the  $\text{HS} \rightarrow \text{LS}_2$  relaxation after irradiation of the  $\text{LS}_2$  phase. All the experiments start from a quantitative population of the HS state at 10 K followed by a relaxation at the indicated temperature.

*Kinetics of the photo-induced HS → LS<sub>2</sub> relaxation after irradiation of the LS<sub>2</sub> phase around T<sub>LIESST</sub>, studied by magnetometry.* Irradiating at higher temperature does not significantly change the relaxation time for a given relaxation temperature. The relaxation curves measured at 45K overlap wherever the irradiation is performed at 10 K or 45 K (Figure S19a). As expected, the lifetime of the irradiated HS<sub>2</sub> is short at 55K, and no complete conversion could be reached (Figure S19b). This suggests that the photogenerated state is the same, whatever the irradiation temperature.

## CONCLUSIONS

The two different thermal transitions previously observed by Real *et al.* with the [Fe(n-Bu-im)<sub>3</sub>(tren)](PF<sub>6</sub>)<sub>2</sub> compound have been confirmed by single crystal optical absorption spectroscopy. The HS→LS relaxation after irradiation has been studied for both LS phases after excitation at 10 K. In both cases, we observed a sigmoidal behavior characteristic of cooperative effects, with a plateau observed only in the HS→LS<sub>1</sub> relaxation. The larger E<sub>o</sub> values obtained for the HS→LS<sub>1</sub> relaxation compared to the HS→LS<sub>2</sub> relaxation (10.2 kJ/mol compared to 3.3 kJ/mol) agrees with the slower dynamics found for the HS→LS<sub>1</sub> relaxation and the thermal stabilization of the LS<sub>2</sub> observed during the thermal spin transition.

For the LS<sub>1</sub> phase we observed two relaxation behavior, depending on the irradiation temperature. Irradiation above 70 K led to unexpected long relaxations time compared to irradiating below 70 K. This was explained by the existence of two different photogenerated HS states: HS<sub>1</sub><sup>1irr</sup> state, whose structure we determined under irradiation at 25 K and the HS<sub>1</sub><sup>2irr</sup> state, whose structure we determined under irradiation of LS<sub>1</sub> at 90 K. The conformations of the butyl chains of the ligand are identical in HS<sub>1</sub><sup>1irr</sup> and in LS<sub>1</sub> state whereas two of the HS<sub>1</sub><sup>2irr</sup> butyl chains adopt a different conformation. Alongside the relaxation, followed by single crystal X-ray diffraction, reorientations of the butyl chains occur through order/disorder transitions. We believe that these reorientations of the butyl chains are responsible for the long relaxation time above 70 K.

Interestingly, a HS<sup>quench</sup> state can also be reached via thermal quenching, with a structure identical to the HS<sub>1</sub><sup>2irr</sup>. The relaxation time of those structurally identical states are of the same order of magnitude.

With the exception of a few Fe-Co charge transfer systems with a cyanide bridge, (Prussian blue analogues) there are only two SCO pure systems that have a T<sub>1/2</sub> above 100 K.<sup>45-46</sup> There are other SCO complexes of Fe (II) that present a T<sub>LIESST</sub> around 90-100 K. However, in the present study, a new type of spin crossover compound is presented: a spin crossover compound with T<sub>LIESST</sub> = 80 K that can be completely populated back to the HS<sub>1</sub> by irradiating at 80 K with a surprisingly high kinetic stability of the photogenerated state.

## ASSOCIATED CONTENT

CCDC files 1848626-1848629 and 1848631 contain the supplementary crystallographic data for this paper. The data can be obtained free of charge from The Cambridge Crystallographic Data Centre via [www.ccdc.cam.ac.uk/structures](http://www.ccdc.cam.ac.uk/structures). Table S8a indicates to

which structure corresponds each deposited cif. These files and additional cif files (see Table S8b) are also available as supporting information.

**Supporting Information.** This material is available free of charge via the Internet at <http://pubs.acs.org>.

## AUTHOR INFORMATION

### Corresponding Author

\* Celine.besnard@unige.ch, \*Jose.A.Real@uv.es

### Author Contributions

All authors have given approval to the final version of the manuscript.

## ACKNOWLEDGEMENT

We are grateful to the Swiss-Norwegian Beamlines (ESRF, Grenoble) for the provision of synchrotron beamtime. Financial support from the Swiss National Science Foundation (Grant No 200020\_152780), the French PIA project "Lorraine Université d'Excellence", reference ANR-15-IDEX-04-LUE, and the CPER, The Spanish Ministerio de Economía y Competitividad (MINECO) (Grants CTQ2016-78341-P and MDM-2015-0538), Generalitat Valenciana (Grant PROMETEO/2016/147), an EU Framework Program for Research and Innovation (RISE project number 734322) are gratefully acknowledged. We are also grateful to Yu Wang for the structures at 25 K of the LS<sub>1</sub> and HS<sub>1</sub><sup>1irr</sup> phases.

## REFERENCES

1. Sato, O., *Nat. Chem.* 2016, 8 (7), 644-656.
2. Bennemann, K. H., *J. Phys. Condens. Matter* 2011, 23 (7), 073202.
3. Shin-ya, K., *J. Phys. Conf. Ser.* 2005, 21 (1), 7.
4. Koenig, E., *Struct. Bonding (Berlin)* 1991, 76 (Complex Chem.), 51-152.
5. Guetlich, P.; Goodwin, H. A.; Editors, *Spin Crossover in Transition Metal Compounds I. [In: Top. Curr. Chem.; 2004, 233]*. Springer-Verlag: 2004; p 341 pp.
6. Halcrow, M. A.; Editor, *Spin-crossover materials: properties and applications*. John Wiley & Sons Ltd.: 2013; p 546 pp.
7. Molnar, G.; Rat, S.; Salmon, L.; Nicolazzi, W.; Bousseksou, A., *Adv. Mater. (Weinheim, Ger.)* 2017, Ahead of Print.
8. Senthil Kumar, K.; Ruben, M., *Coord. Chem. Rev.* 2017, 346, 176-205.
9. Kahn, O.; Martinez, C. J., *Science (Washington, D. C.)* 1998, 279 (5347), 44-48.
10. Prins, F.; Monrabal-Capilla, M.; Osorio, E. A.; Coronado, E.; van der Zant, H. S. J., *Adv. Mater.* 2011, 23 (13), 1545-1549.
11. Ohba, M.; Yoneda, K.; Agusti, G.; Munoz, M. C.; Gaspar, A. B.; Real, J. A.; Yamasaki, M.; Ando, H.; Nakao, Y.; Sakaki, S.; Kitagawa, S., *Angew. Chem., Int. Ed.* 2009, 48 (26), 4767-4771, S4767/1-S4767/16.
12. Salmon, L.; Molnar, G.; Zitouni, D.; Quintero, C.; Bergaud, C.; Micheau, J.-C.; Bousseksou, A., *J. Mater. Chem.* 2010, 20 (26), 5499-5503.
13. Matsuda, M.; Kiyoshima, K.; Uchida, R.; Kinoshita, N.; Tajima, H., *Thin Solid Films* 2013, 531, 451-453.

14. Shepherd, H. J.; Gural'skiy, I. y. A.; Quintero, C. M.; Tricard, S.; Salmon, L.; Molnar, G.; Bousseksou, A., *Nat. Commun.* 2013, **4**, 3607/1-3607/9.
15. Decurtins, S.; Guetlich, P.; Koehler, C. P.; Spiering, H.; Hauser, A., *Chem. Phys. Lett.* 1984, **105** (1), 1-4.
16. Hauser, A.; Vef, A.; Adler, P., *J. Chem. Phys.* 1991, **95** (12), 8710-17.
17. Hauser, A., *Comments Inorg. Chem.* 1995, **17** (1), 17-40.
18. Letard, J.-F., *J. Mater. Chem.* 2006, **16** (26), 2550-2559.
19. Collet, E.; Guionneau, P., *C. R. Chim.* 2018.
20. Matouzenko, G. S.; Luneau, D.; Molnár, G.; Ould-Moussa, N.; Zein, S.; Borshch, S. A.; Bousseksou, A.; Averseng, F., *Eur. J. Inorg. Chem.* 2006, **2006** (13), 2671-2682.
21. Koenig, E.; Ritter, G.; Kulshreshtha, S. K.; Nelson, S. M., *Inorg. Chem.* 1982, **21** (8), 3022-3029.
22. Matouzenko, G. S.; Bousseksou, A.; Borshch, S. A.; Perrin, M.; Zein, S.; Salmon, L.; Molnar, G.; Lecocq, S., *Inorg. Chem.* 2004, **43** (1), 227-236.
23. Money, V. A.; Elhaik, J.; Radosavljevic Evans, I.; Halcrow, M. A.; Howard, J. A. K., *Dalton Trans.* 2004, (1), 65-69.
24. Chernyshov, D.; Hostettler, M.; Tornroos, K. W.; Burgi, H.-B., *Angew. Chem., Int. Ed.* 2003, **42** (32), 3825-3830.
25. Koenig, E.; Ritter, G.; Kulshreshtha, S. K.; Waigel, J.; Sacconi, L., *Inorg. Chem.* 1984, **23** (9), 1241-1246.
26. Wu, C.-C.; Jung, J.; Gantzel, P. K.; Gütlich, P.; Hendrickson, D. N., *Inorg. Chem.* 1997, **36** (23), 5339-5347.
27. Hostettler, M.; Törnroos, K. W.; Chernyshov, D.; Vangdal, B.; Bürgi, H.-B., *Angew. Chem.* 2004, **116** (35), 4689-4695.
28. Miyazaki, Y.; Nakamoto, T.; Ikeuchi, S.; Saito, K.; Inaba, A.; Sorai, M.; Tojo, T.; Atake, T.; Matouzenko, G. S.; Zein, S.; Borshch, S. A., *J. Phys. Chem. B* 2007, **111** (43), 12508-12517.
29. Kusz, J.; Zubko, M.; Neder, R. B.; Guetlich, P., *Acta Crystallogr., Sect. B: Struct. Sci.* 2012, **68** (1), 40-56.
30. Sheu, C.-F.; Pillet, S.; Lin, Y.-C.; Chen, S.-M.; Hsu, I. J.; Lecomte, C.; Wang, Y., *Inorg. Chem.* 2008, **47** (23), 10866-10874.
31. Sereidyuk, M.; Muñoz, M. C.; Castro, M.; Romero-Morcillo, T.; Gaspar, A. B.; Real, J. A., *Chem. Eur. J.* 2013, **19** (21), 6591-6596.
32. <https://www.rigaku.com/en/products/smc/crysalis>.
33. Dolomanov, O. V.; Blake, A. J.; Champness, N. R.; Schroeder, M., *J. Appl. Crystallogr.* 2003, **36** (5), 1283-1284.
34. Sheldrick, G., *Acta Crystallogr. C* 2015, **71** (1), 3-8.
- 35 <http://www.esrf.eu/home/UsersAndScience/Experiments/CRG/BM01/bm01/image.htm/snbl-tool-box.html>.
36. Coelho, A., 2007.
37. Otwinowski, Z.; Minor, W., [20] Processing of X-ray diffraction data collected in oscillation mode. In *Methods in Enzymology*, Academic Press: 1997; Vol. 276, pp 307-326.
38. Pillet, S.; Legrand, V.; Souhassou, M.; Lecomte, C., *Phys. Rev. B* 2006, **74** (14), 140101.
39. Landau, L.; Lifshitz, E.; Shoenberg; Editors, *Statistical Physics*. Oxford Univ. Press: p 234 pp.
40. Mariette, C.; Trzop, E.; Zerdane, S.; Fertey, P.; Zhang, D.; Valverde-Munoz, F. J.; Real, J.-A.; Collet, E., *Acta Crystallogr., Sect. B: Struct. Sci., Cryst. Eng. Mater.* 2017, **73** (4), 660-668.
41. Hauser, A.; Enachescu, C.; Daku, M. L.; Vargas, A.; Amstutz, N., *Coord. Chem. Rev.*, **250** (13-14), 1642-1652.
42. A rapid cooling of the sample freezes the HS state at low temperature and the lack of control of the temperature of a helijet-type cooling device above 60 K hampered obtaining the LS1 phase at 10 K. We therefore used another cooling device with lowest possible temperature of 25 K.
43. The nominal temperature indicated by the cryostream was 80 K. However, the sample the temperature was lower and was determined to be around 90 K by comparison with the spectroscopic measurements.
44. Hauser, A.; Jeftić, J.; Romstedt, H.; Hinek, R.; Spiering, H., *Coord. Chem. Rev.* s 1999, **190-192**, 471-491.
45. Marcén, S.; Lecren, L.; Capes, L.; Goodwin, H. A.; Létard, J. F., *Chem. Phys. Lett.* 2002, **358** (1), 87-95.
46. Costa, J. S.; Balde, C.; Carbonera, C.; Denux, D.; Wattiaux, A.; Desplanches, C.; Ader, J.-P.; Gütlich, P.; Létard, J.-F., *Inorg. Chem.* **2007**, **46** (10), 4114-4119.